1. ACCEPTANCE

1.1 Theory

The definition of an acceptance, A, is as follows:

$$A = \frac{N_{pass}}{N} \tag{1.1}$$

where N is the total number of events produced in the collision and N_{pass} is the number of these passing the event selection. For statistical purposes, the data used in this analysis is filtered by the means of generator level cuts so only events likely to pass the event selection **??** are in the input files. Thus a filter efficiency referring to the rejection power of the generator cuts must be included and equation 1.2 becomes:

$$A = \frac{N_{pass}}{N_{sample}} \times \epsilon_{fil} \tag{1.2}$$

where N_{sample} is the number of events in the data set and ϵ_{fil} is the filter efficiency of the sample. This number is given by the Monte Carlo production group, 0.88 and 0.96 for the W and Z Pythia samples respectively.

Table 1.1 shows the rejection power of the event selection on the truth level quantities. The electrons used already account for bremsstrahlung effects. The end result after all cuts multiplied by the filter efficiency is, to first order, the acceptance.

Cut	Z detail	% Z remaining	W detail	% W remaining
Electron P_T	$\times 2$	61.74 (0.31)	$\times 1$	72.53 (0.34)
Electron η	$\times 2$	36.53 (0.22)	$\times 1$	63.15 (0.31)
	+ Z Mass cuts	32.28 (0.20)	+ MEt	51.34 (0.27)
Overall acceptance		27.76 (0.20)		32.35 (0.27)

Tab. 1.1: Impact of selection cuts on acceptance values. Statistical uncertainty given in parentheses.

1.2 Binned acceptances

For the purposes of a differential cross section measurement with respect to variable x, in the interests of consistency, one must take the acceptances binned also in x. Figures 1.2 show the variation of acceptance with boson P_T and η. It is seen that the acceptance decreases fairly

steadily with increasing η. The reason for this is that a forward boson with high pseudo-rapidity will tend to decay into two electrons also with high values of η, which are more likely to fail the selection cut of electron $|\eta|$ <2.4. The explanation for the behaviour with respect to boson P_T (the drop in acceptance at middle values of P_T and subsequent increase in acceptance as P_T is increased further) is more complex and as follows (consider for simplicity η=0):

- **Zero boson P_T region** (figure 1.1(a)): At zero boson transverse momenta, by conservation of momenta the two decay electrons must be monoenergetic and back to back
- **Low boson P_T region** (figure 1.1(b)): As boson transverse momenta increases slightly, by conservation of momenta the two decay electrons become less monoenergetic. Thus one is more likely to fail the 25 GeV P_T threshold cut and the acceptance will decrease.
- **Medium boson P_T region** (figure 1.1(c)): As boson transverse momenta increases further, at some threshold (at about 45 GeV) the decay electrons will cease to be back to back and will start decaying in the same direction.
- **High boson P_T region** (figure 1.1(d)): At high boson transverse momenta increases yet further, the electrons will have higher P_T and the acceptance will increase.

Obviously, the more bins the better but it is of vital importance that sufficient events are in each bin so that the statistical uncertainty of both the numerator and denominator in that bin is under control, otherwise cross sections in certain bins may be wildly mis-calculated (which also has a significant impact on the calculation of a global as well as differential cross section!). The binning chosen is shown in figure 1.4, for $Z \rightarrow ee$ only as these have less events in each bin (as η binning is not used for $W \rightarrow e\nu$ events: η is not reconstructed in these due to no measurement on η of the neutrino).

1.3 Acceptance corrections

1.3.1 Acceptance and M_Z

Due to the generator level cuts, the denominator of the calculated acceptance includes Drell Yann down to M_Z=60 GeV. It is important at this point to emphasise the difference between M_Z and M_{ee}: M_Z is the generator level mass of the Z boson, where M_{ee} is the invariant mass of the two generator level electrons in the event. The lineshapes look slightly different at low M_Z due to imperfections in the photon merging procedure required when computing M_{ee} (see next

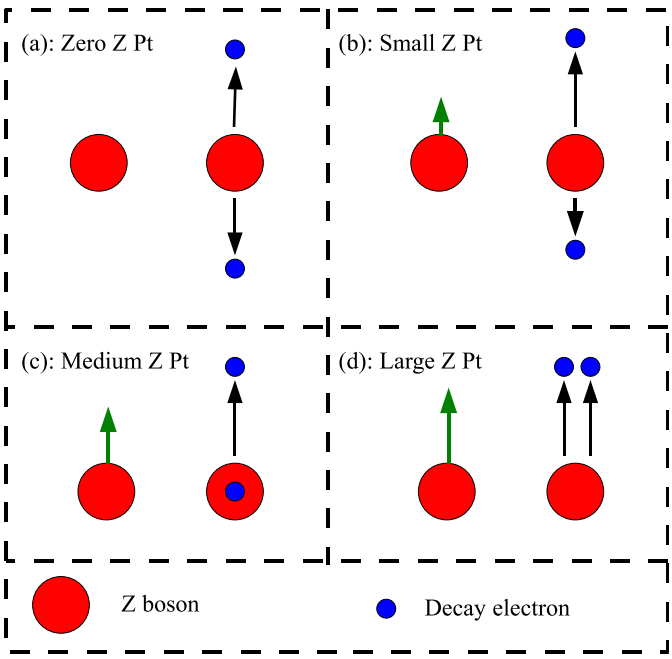

Fig. 1.1: Relation of boson and electron transverse momenta

section).

The threshold of the low mass cut at 60 GeV is somewhat arbitrarily chosen when the PYTHIA samples were generated, and to estimate the impact of this cut on the acceptance, the cut was varied between 60 and 70 GeV (thus altering the denominator in the acceptance equation), and the results are shown in figure 1.5 [1]. Superimposed on the graph is the truth Z lineshape at that value of M_Z.

It is observed that the acceptance increases linearly by an amount ∼0.1% for each 1 GeV increase in the lower threshold cut. The reason for this is that a higher mass cut will decrease the denominator but not the numerator (which has implicit Z peak cuts between 80 and 100 GeV). The purpose is to strike a balance between purity and efficiency of Z (as opposed to photon) propagators. Thus the cut used for a cross section analysis was chosen to lie at the minimum of the Z lineshape (red) curve, at 67 GeV. However this choice is somewhat arbitrary and thus a

[1] the acceptance values are lower than the usual quoted values in this graph as photon merging has not been performed when obtaining these values

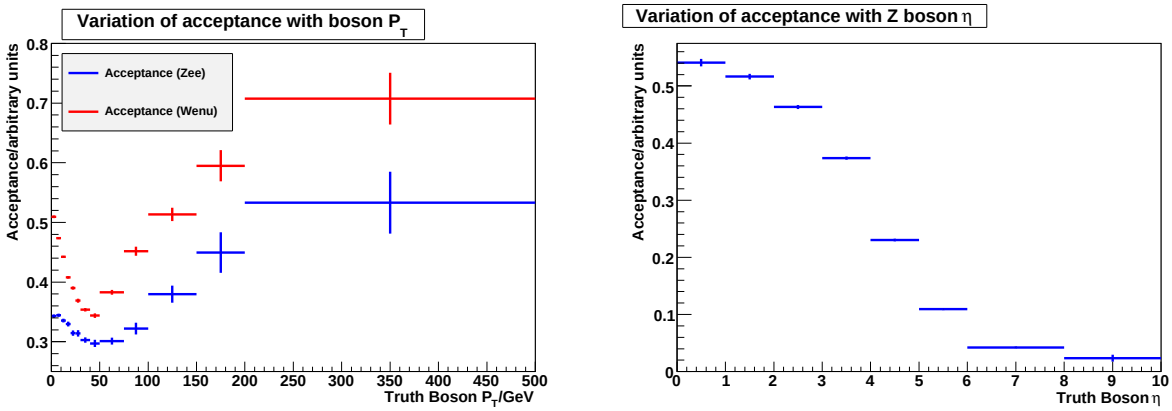

(a) Acceptance variation with boson P_T

(b) Acceptance variation with boson η

Fig. 1.2: Acceptances with respect to boson kinematic variables. Acceptances shown without filter efficiencies included.

systematic of 0.5% (the approximate variation of acceptance between a lower mass cut of 60 and 70 GeV) is attributed to this choice.

1.3.2 Photon merging

All photons with a parent ID of the boson need to be merged into the electrons. The number and P_T spectra of such photons is shown in figures 1.6(a) and 1.6(b). Figure 1.6(a) shows that merging is necessary in about 50% of events. The impact of a photon merging is to increase the electron Pt values and thinning the Z mass peak, as may be seen in figure 1.6(b) and 1.6(c).

The merging is performed by adding the Lorentz vectors of any photons within a certain ΔR distance to the closest truth electron to the photon. Figure 1.6(d) shows the ΔR distance between all direct photons and electrons in the event. There is no clear minima in this distribution so it is not clear where to put the merging cut. A solution was found experimentally, by examining the Z mass peak for different ΔR values.

Figure 1.6(e) shows (in black) the 'correct Z mass' peak, that is to say, that obtained directly from the generation properties of the Z boson. This could in theory be used for acceptance calculation but there would be systematic differences resulting as, obviously, in the real data (which the acceptance is trying to model), one must cut on the peak obtained by calculating the invariant mass of the two electrons. The coloured mass peaks are those obtained as such, as in, those obtained from the two truth electrons in the event when merged with truth photons in the event.

The variation between peaks is due to the ΔR cut being varied. The fewer the number of

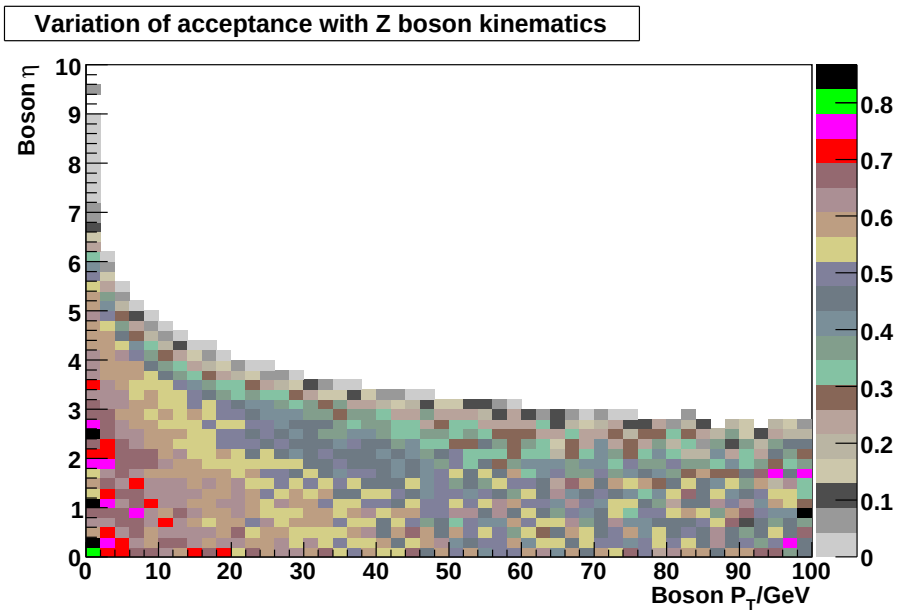

Fig. 1.3: Acceptances with respect to both boson P_T and η, as to be folded into the cross section analysis. Acceptances shown without filter efficiencies included.

events *below* the threshold cut of 60 GeV, the more successful the merging. That is to say, the aim is to make the peak reconstructed from electrons to look as similar as possible to the peak obtained from the Z boson itself. This is seen from the graph to be at a ΔR cut of about 2.5.

Figure 1.6(f) shows this a little more quantitively. It displays the calculated acceptance with different ΔR cuts. It is seen that the acceptance is low with low ΔR cut (where the electron P_T spectra is lowered as insufficient merging is being done) and raises up to a plateau at $\Delta R \simeq 2$. The acceptance does not lower again (even with no ΔR cut), and thus in the analysis no cut was used and all truth photons originating from a Z are simply merged into the closest electron.

Because all objects in the event are now accounted for, the Z mass peak becomes thinner. The overall impact on the acceptance is to increase it as a consequence of the increased electron Pt values. The modification to acceptance value due to photon merging, with the parameters optimised as above, is found to be 1.53% for W events and 1.47% for Z events.

1.3.3 Resolution corrections

The acceptance is calculated by running the truth level quantites through the event selection. However, in the case of a data drived measurement, it is the reconstructed quantities to which these cuts are actually implemented. Thus a correction truth→reconstructed must be made. It is

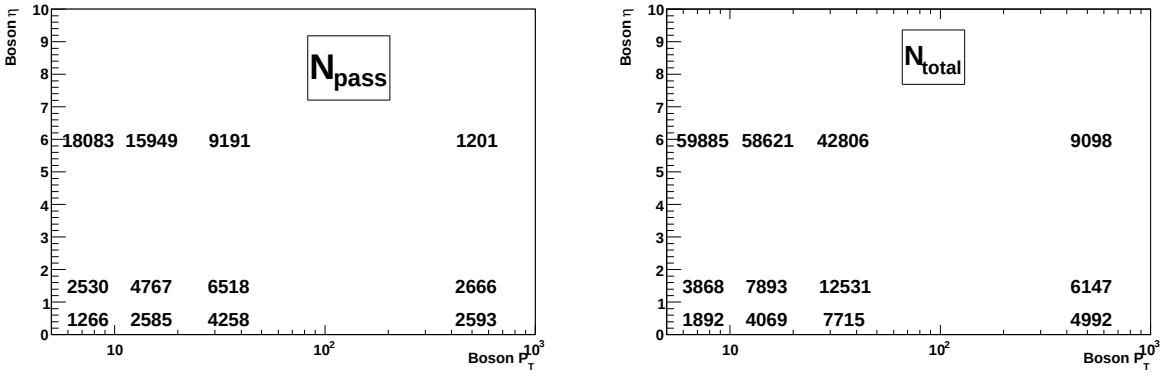

Fig. 1.4: Number of events in each bin chosen for a $100\,\mathrm{pb}^{-1}$ analysis. $Z \rightarrow ee$ results only are shown.

not possible to simply apply the event selection on the reconstructed quantites in the Monte Carlo data sets to obtain rejection factors as baseline quantities (such as minimum transverse momenta on a reconstructed electron being about 5GeV; below this soft electrons make reconstruction very difficult CITE); would distort the acceptance value. Thus resolution functions mapping truth to reconstructed values are used. Ideally these need to be determined from data, and studies on how to obtain these are detailed in chapter **??**. The strategies explored to determine acceptance corrections are as follows:

Methodology

General smearing technique

The methodology is split up into two loops summarised in figure 1.7: the first to obtain resolution functions (a Monte Carlo based Reco-Truth resolution function and its data driven equivalent), and the second to smear the truth values using a random number generated from the resolution function (as opposed to using a Gaussian fit of the function, which in the case of electron smearing causes an unacceptable variation in acceptance due to the non-Gaussian tails of the resolution function). It must be noted that the resolution functions are binned in an appropriate variable, the choice of which will be explained in greater detail.

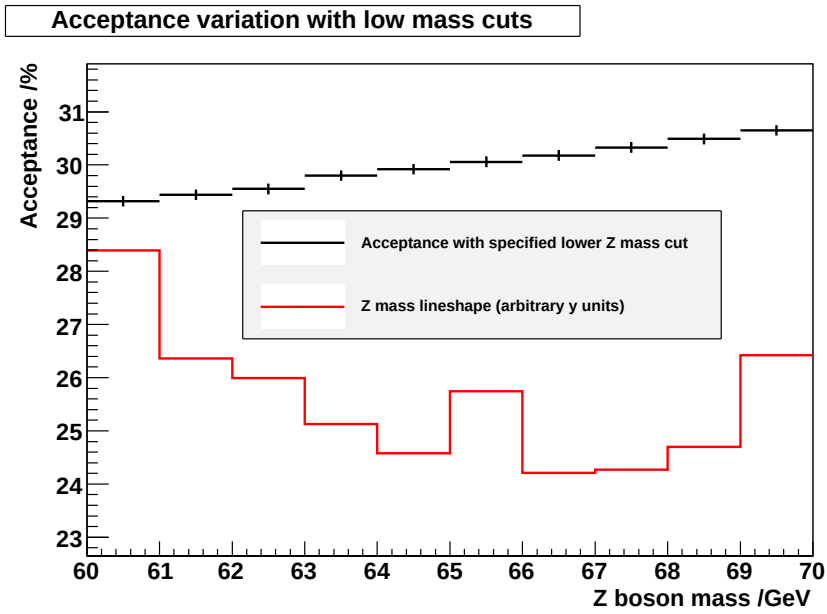

Fig. 1.5: Variation of acceptances as lower mass cut is varied. The Z mass lineshape (in red) is superimposed (scaled to arbitrary y units)

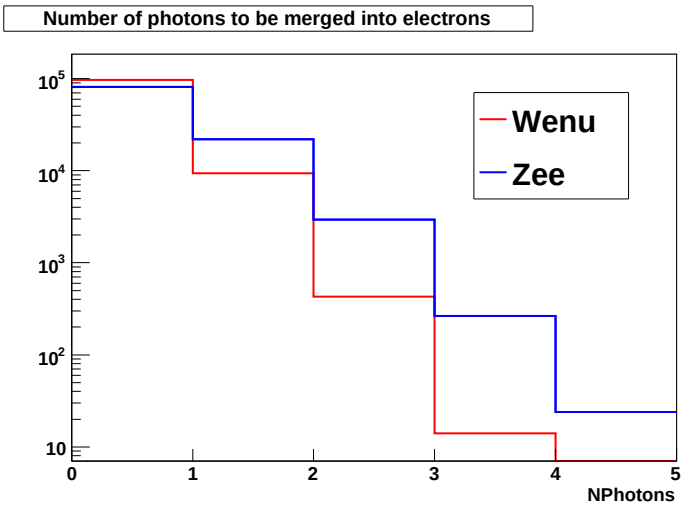

(a) Number of photons to be merged into the electrons in both W and Z events

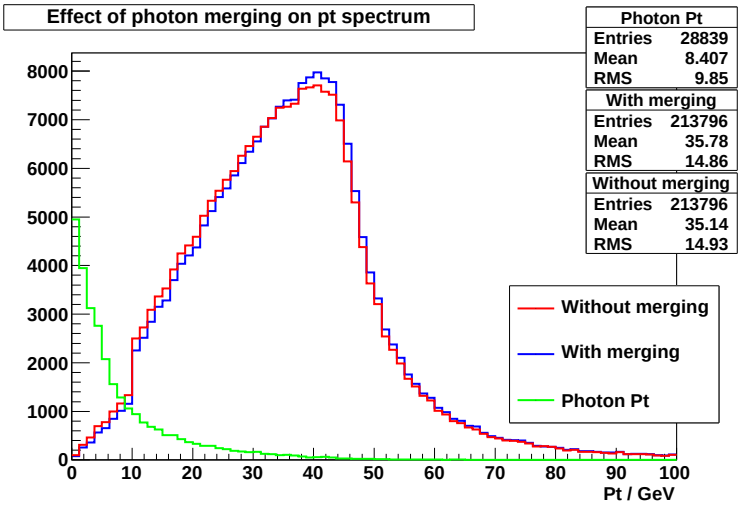

(b) Impact of photon merging on electron Pt spectrum. Photon Pt spectrum also shown in green.

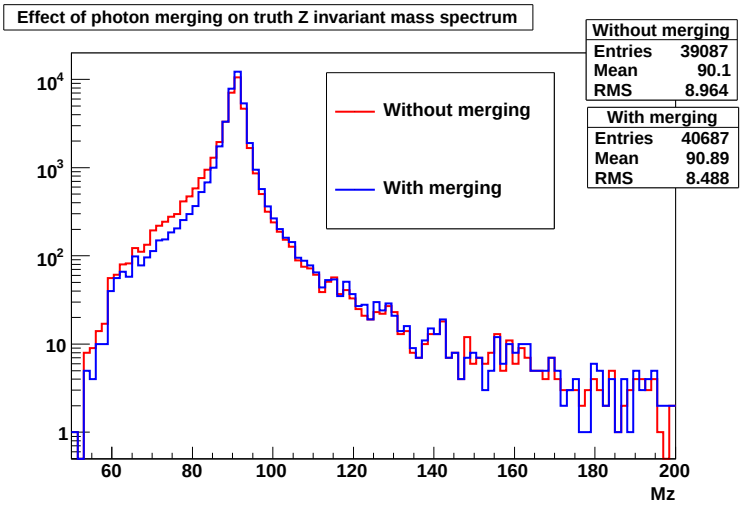

(c) Impact of photon merging on Z mass peak

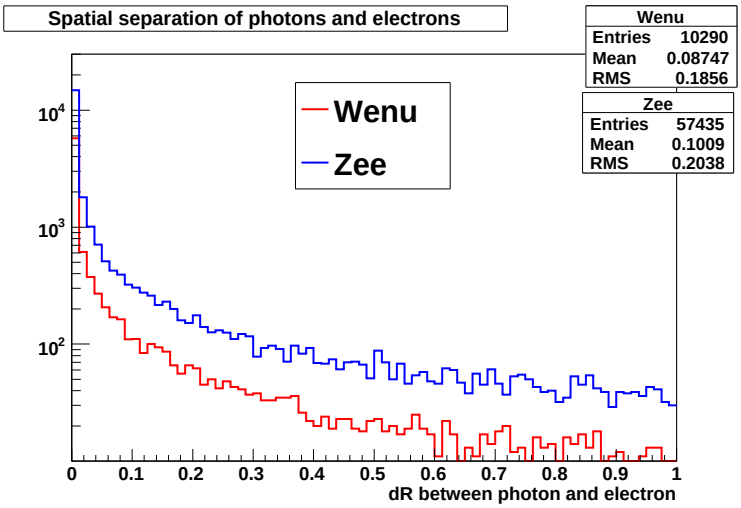

(d) dR distribution of photons to be merged into the electrons in both W and Z events

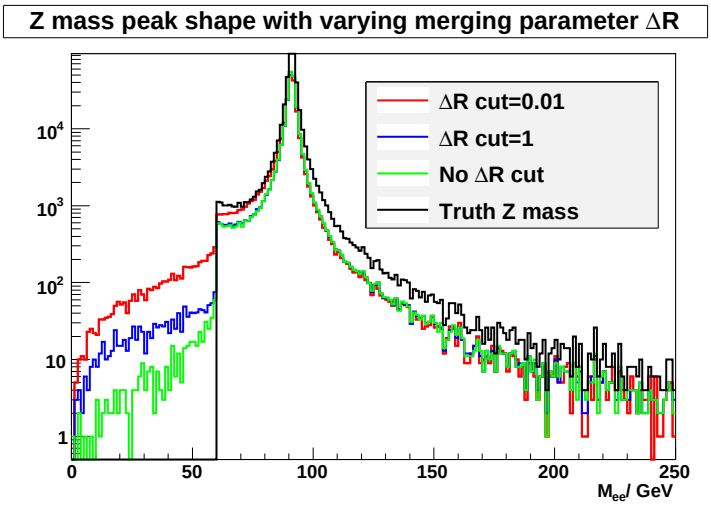

(e) Impact of photon merging cut on the Z invariant mass spectrum.

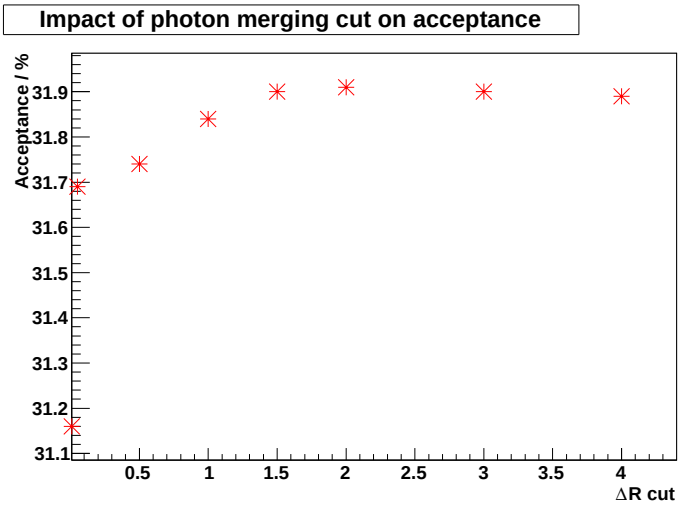

(f) Calculated acceptance with varying ΔR cut

Fig. 1.6: Impact of photon merging Z mass peak and calculated acceptance

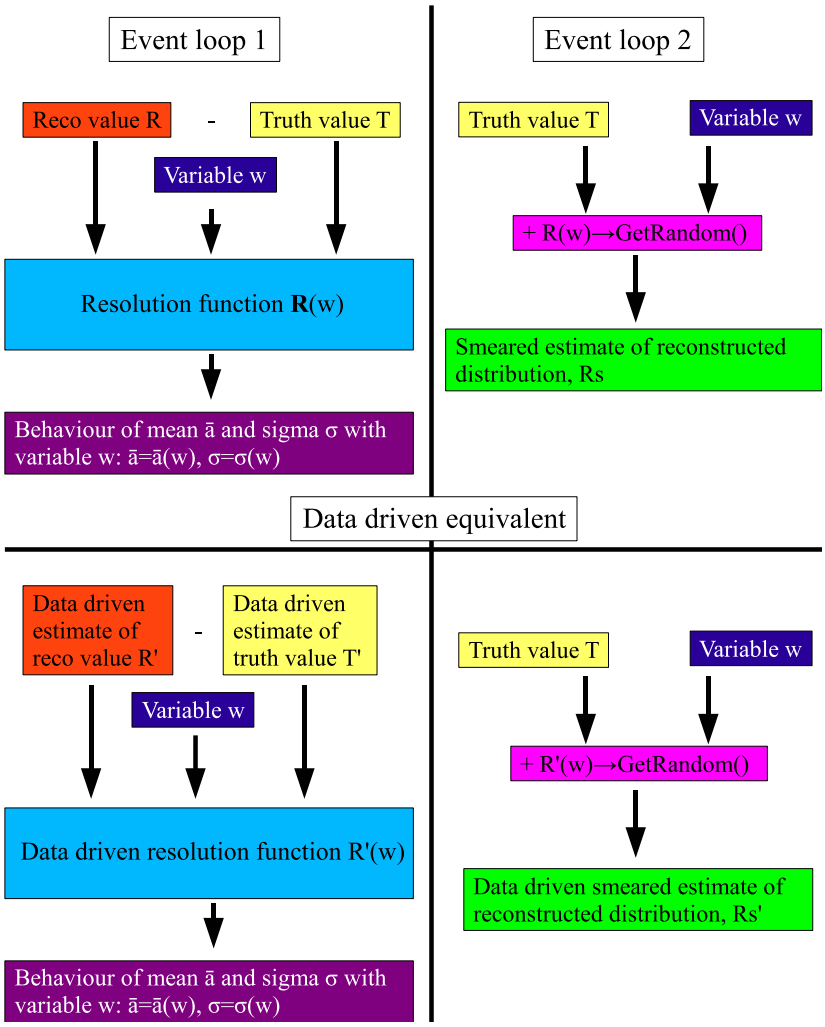

Fig. 1.7: Smearing methodology. Note the definition of the distributions **R**, **T** and $\mathbf{R_s}$.

Magnitude smearing

The $\not\!\!E_t$ magnitude of the object is smeared, as is seen in figure 1.8 by a resolution function, that is, to perform a scalar transformation. The resolution function is determined by |reco P_T|-|truth P_T|, or a data driven equivalent.

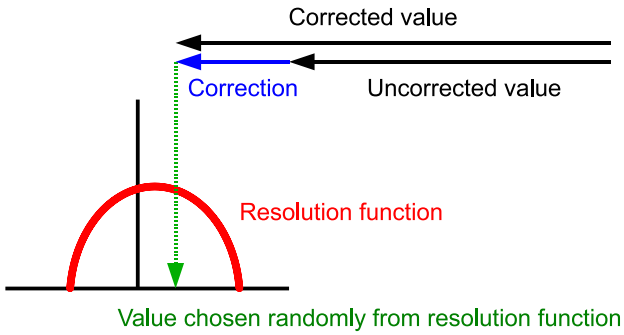

Fig. 1.8: Smearing methodology (a)- scalar

Component smearing

The p_t vector of the object is resolved along two chosen axes (in figure 1.9(a) the x and y axes are chosen for demonstration but in reality it could be any) and resolution smearing is performed along these axes. The resolution functions must be the correct function *along that particular axis*. The smeared components are then recombined to obtain an overall smeared p_t using the following procedure (the directions parallel and perpendicular to the ZP_T direction are chosen for demonstration, and the quantities are defined in figure 1.9(a)).

The components of $\not\!\!E_t$ parallel and perpendicular to the Z P_T direction (Z(P_T) and AZ(P_T) are given as follows:

$$\not\!\!E_t{}^Z = \not\!\!E_t \cdot Z(P_T) = |\not\!\!E_t| \cos\alpha, \tag{1.3}$$

$$\not\!\!E_t{}^{AZ} = \not\!\!E_t \cdot AZ(P_T) = |\not\!\!E_t| \sin\alpha, \tag{1.4}$$

It is these quantities which are smeared, altering both the angle and the magnitude of the $\not\!\!E_t$

vector:

$$\not{E}_{tZ}{}' = |\not{E}_t'| \cos\alpha', \tag{1.5}$$
$$\not{E}_{tAZ}{}' = |\not{E}_t'| \sin\alpha', \tag{1.6}$$

where

$$\not{E}_t' = \sqrt{(\not{E}_{tZ}{}')^2 + (\not{E}_{tAZ}{}')^2} \tag{1.7}$$

The components of the smeared $\not{E}_t$ vector along the x and y axes are given by

$$P_x = \not{E}_t' \cos\theta' \tag{1.8}$$
$$P_y = \not{E}_t' \sin\theta' \tag{1.9}$$

where from the diagram it can be seen by inspection that

$$\theta' = \alpha' - \alpha + \theta \tag{1.10}$$

Thus the smeared met vector, $\not{E}_t$ ' may be obtained.

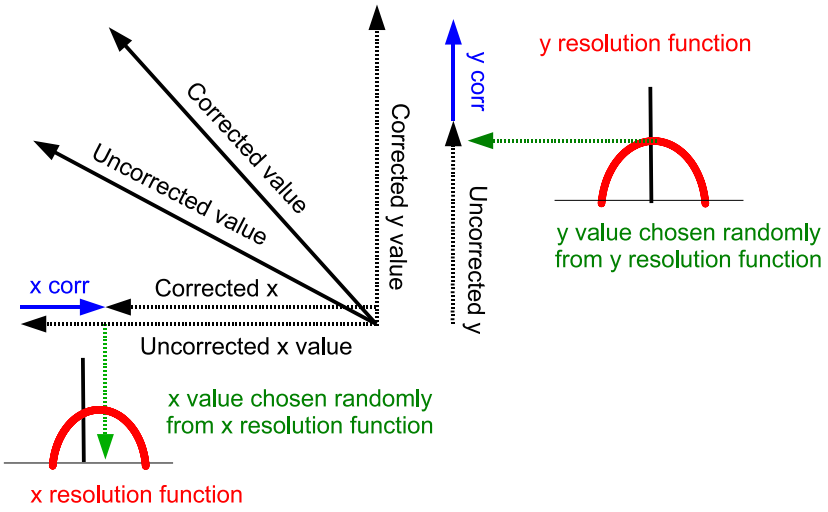

(a) Smearing a quantity along component axes.

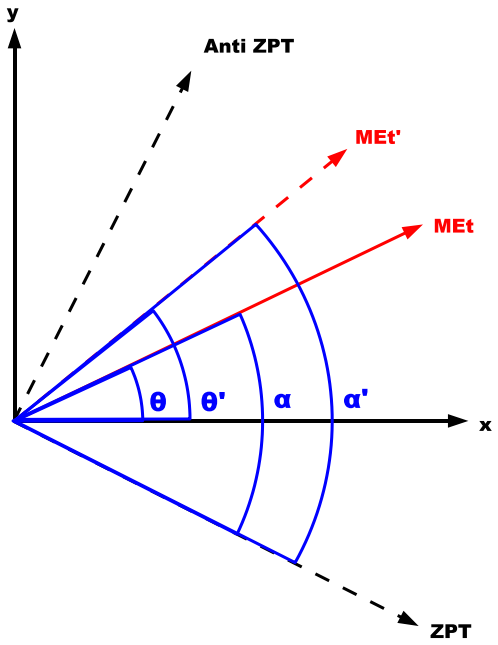

(b) Recombination of a quantity smeared along component axes.

Fig. 1.9: Smearing methodology (b)- resolving along axes

Smearing electron Pt

The appropriate variable to bin both the electron P_T scales and resolutions is the electron P_T itself, as may be seen in figure **??**. As the electron resolution is approximately 3GeV, 50 bins were chosen over the range 0-150 GeV. Figure 1.10 shows the electron P_T **T**, **R** and $\mathbf{R_s}$ distributions (in $W \rightarrow e\nu$ events, although similar results are seen in $Z \rightarrow ee$) as per the procedure described in figure 1.7. The left plot has some considerable bias between **R** and $\mathbf{R_s}$, particularly at low P_T. This is due to the variation of the trigger and reconstruction efficiencies with **R**, which is particularly noticeable at low P_T due to the turn on curve. This has to be corrected for when comparing truth and reconstructed electron quantities by folding in the total efficiency dependency on the electron p_t to **T**. We see in figure 1.11 that the smearing procedure produces a distribution much close to **R** than the unsmeared distribution **T**.

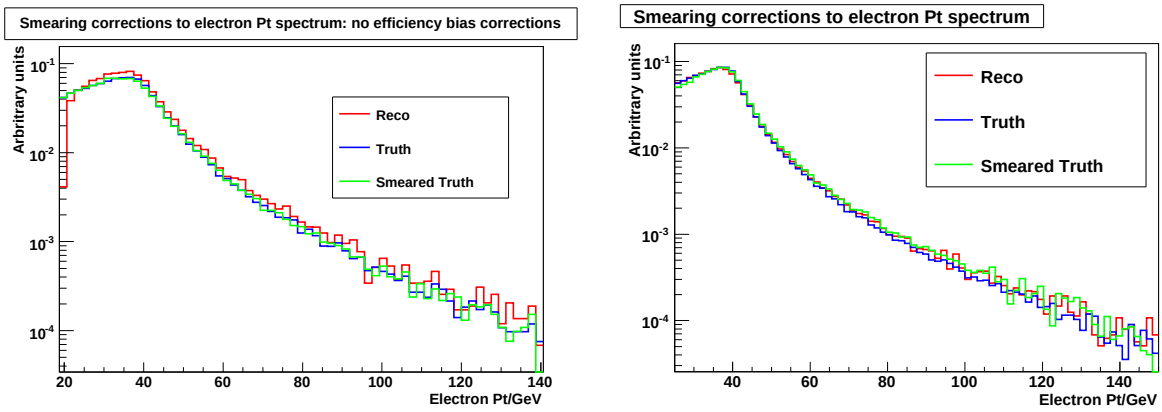

Fig. 1.10: Electron P_T distributions in $W \rightarrow e\nu$ events before and after smearing procedure. Effect of correcting for the trigger and reconstruction bias is shown in the plot on the right

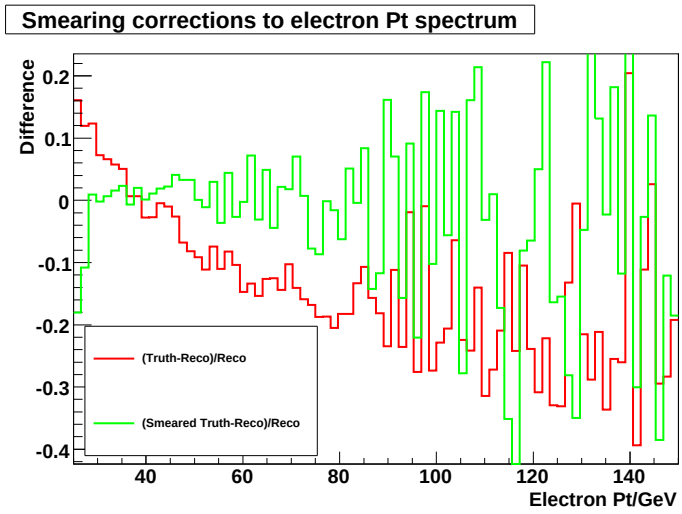

Fig. 1.11: Residual differences between $\mathbf{R_s}$ and $\mathbf{R}$ (green). Initial difference between $\mathbf{R}$ and $\mathbf{T}$ is shown for comparison in red.

Smearing MEt

MC study in release 13

A study into the use of the smearing technique is demonstrated in Athena release 13. It is for demonstration purposes only and the final release 14 results will be shown in subsequent chapters.

A parallel technique as to the electrons was attempted on the $\not\!\!E_t$ distributions, where the scales and resolutions were binned in terms of hadronic activity. The resultant distributions are shown in figure 1.12. It must be noted that no efficiency correction has been made in these distributions. There are two worrying aspects of this plot. The first being that **R** and **T** lie almost on top of each other. The second is that $\mathbf{R_s}$ lies very far away from **R**.

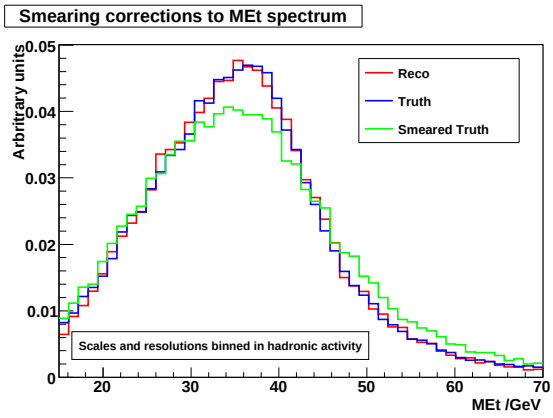

Fig. 1.12: $\not\!\!E_t$ distributions in $W \rightarrow e\nu$ events before and after smearing procedure.

Chapter **??** has told us that the $\not\!\!E_t$ resolution is approximately 3GeV, although dependent upon hadronic activity and the size of the $\not\!\!E_t$itself. The $\not\!\!E_t$scale bias ranges down to about -3GeV, (ignoring the effect at very low $\not\!\!E_t$ as this is far below the cut for $W \rightarrow e\nu$ event selection in any case). Plot 1.13 shows us a toy Monte Carlo study, smearing **T** on an event by event basis by a random number generated from Gaussian functions of the form G($\overline{x}$, σ)=G(0, 6) and G(-3, 0.01). We see that a Gaussian function with σ=6 will smear the $\not\!\!E_t$ distribution much more than what is observed in **R** in figure 1.12. Indeed, if another toy Monte Carlo study is used to manually smear **T** with a random number generated from a Gaussian function, the σ value found to allow $\mathbf{R_s}$ to lie on top of **R** is less than 1GeV, clearly much smaller than the known ATLAS $\not\!\!E_t$resolution.

Figure 1.14 demonstrates a theory as to how this has occurred. Given that the peak is *Jacobian*, and thus asymmetric, smearing will flatten the peak as usual but in bias towards the steep side of the peak (in the diagram shown this is on the right). If a negative scale bias is also

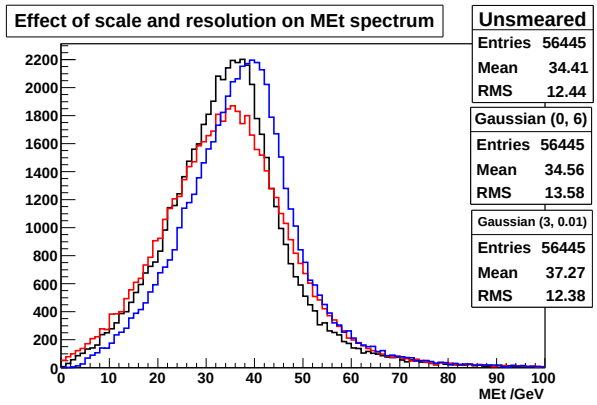

Fig. 1.13: EtMiss distributions in wenu events smeared using a random number generated from a Gaussian function with parameters as defined in the statistics boxes.

present, as is the case in $\not\!\!E_t$ scale, this may to some extent cancel out the effect of resolution and the final scaled and smeared distribution may, in the case of unfortunate coincidence, lie very close to the original distribution.

To test this hypothesis, one must separate out the effects of scale and resolution which have, in the case of $\not\!\!E_t$, been seen to depend on different variables. Independent corrections must be applied for scale and resolution to $\mathbf{T}$ and a strategy for doing so is outlined in figure 1.15.

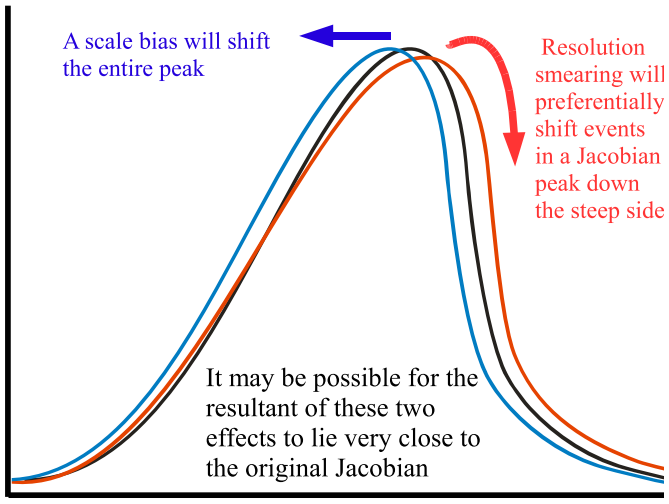

Fig. 1.14: Effect of resolution and scale bias on a Jacobian peak

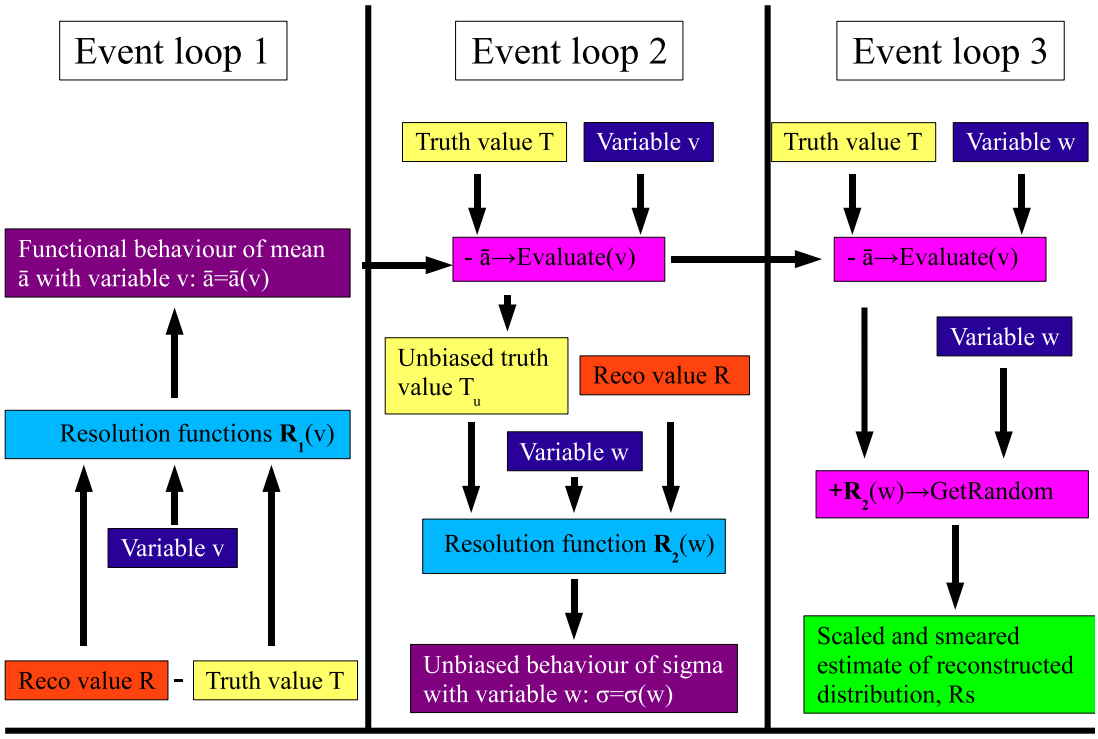

Fig. 1.15: Strategy to apply unbiased corrections of scale and resolution to truth value. Note the definitions of variables v and w.

One must carefully choose variables v and w so that an accurate scale and smearing is applied. In chapter **??** it was seen that the sensible variable to use for resolution is the hadronic activity, as seen in figure **??**. The correct variable for scale is either the magnitude of the $\not\!\!E_t$ itself (as may be seen in figure **??**) or the hadronic recoil when resolved along the axis of the boson transverse momenta (as may be seen in figure **??**). Figure 1.16 shows the smeared distributions when the variables are binned in these variables. We see in these cases **R** is successfully recovered. **Data**

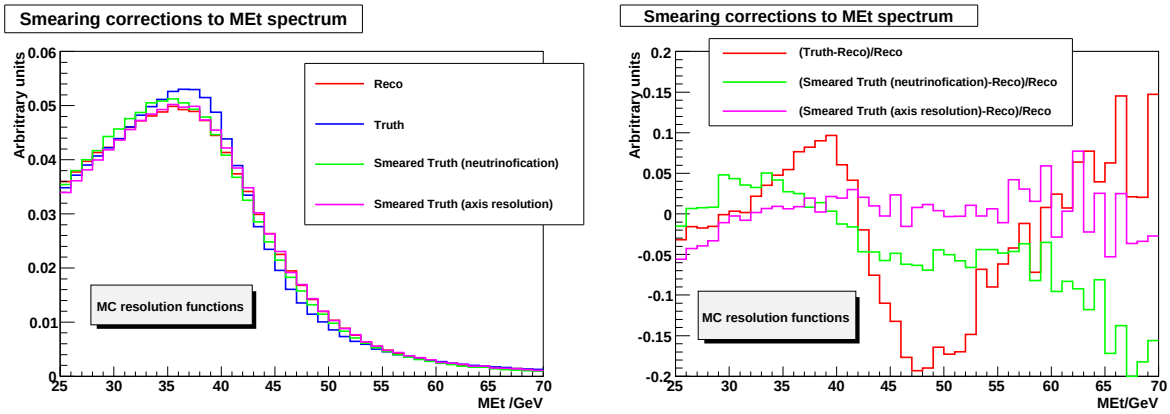

(a) Impact of $\not\!\!E_t$ smearing on spectrum

(b) Corrections to truth $\not\!\!E_t$ distribution from smearing

Fig. 1.16: **T**, **R** and $\mathbf{R_s}$ for $\not\!\!E_t$ (data driven techniques)

driven comparison

A similar exercise was carried out using resolution functions derived from data driven methods. Two methods were explored, following the procedure shown in figure 1.15:

- Procedure a:
  $\Rightarrow$ $\not\!\!E_t$ in a $Z \rightarrow ee$ event resolved along the parallel and perpendicular axes to obtain $\overline{a}$(v) and σ(w) where v=hadronic recoil and w=hadronic activity.
  $\Rightarrow$ Truth $\not\!\!E_t$ in a $W \rightarrow e\nu$ event scaled and smeared as according to these values.

- Procedure b:
  $\Rightarrow$ Neutrinofication in a $Z \rightarrow ee$ event performed to obtain $\overline{a}$(v) and σ(w) where v=$|\not\!\!E_t|$ and w=hadronic activity.
  $\Rightarrow$ Truth $\not\!\!E_t$ in a $W \rightarrow e\nu$ event scaled and smeared as according to these values.

Figure 1.17 shows the resultant $\not\!\!E_t$ distributions from these procedures. Good agreement is shown.

MC study in release 14

The resultant smeared distributions for $\not\!\!E_t$ are shown in figure **??**.

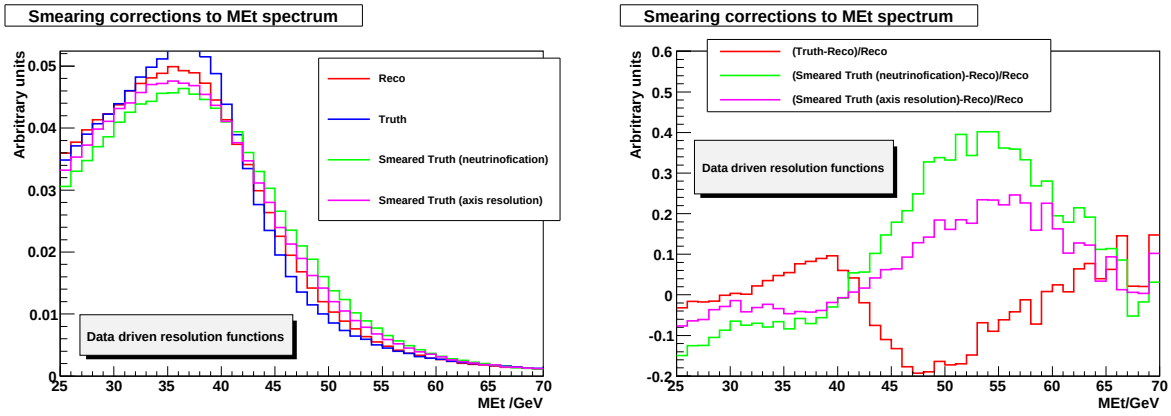

(a) Impact of $\not\!\!E_t$ smearing on spectrum

(b) Corrections to truth $\not\!\!E_t$ distribution from smearing

Fig. 1.17: **T**, **R** and $\mathbf{R_s}$ for $\not\!\!E_t$ (data driven techniques)

1.3.4 Results

Final impact of acceptances

The event selection code (cuts at 25GeV on both electrons and $\not\!\!E_t$) was then run on the unmodified quantities (electron p_t and $|\not\!\!E_t|$), and the quantities after smearing. Table 1.2 shows these computed quantities. The following observations were made:

- The effect of electron smearing is larger in $Z \rightarrow ee$ events (about 1.1%) than for $W \rightarrow e\nu$ (0.7%). This is hardly surprising, as there are twice the number of electrons in $Z \rightarrow ee$ than in $W \rightarrow e\nu$ events.

- It may be seen that, for $W \rightarrow e\nu$ events, the smearing correction in $\not\!\!E_t$ ($\sim 0.1\%$) is a smaller correction than for the electron correction ($\sim 0.7\%$). This is not a reflection of the larger scale bias and resolution in $\not\!\!E_t$ than for electrons, but it due to the 'unfortunate cancelling' of the scale and resolution in this particular $W \rightarrow e\nu$ sample, leading to the truth and reconstructed distributions lying very close to each other.

- The systematic on $\not\!\!E_t$ smearing evaluated from the difference in acceptance between MC and data driven smearing is seen to be 0.3% for both procedures a and b. Thus an overall systematic of 0.3% on using data driven smearing functions was chosen.

- The systematic on $\not\!\!E_t$ smearing evaluated from the difference in acceptance between procedure a and b is seen to be 0.04%. Thus a 0.04% systematic was chosen on the $\not\!\!E_t$ smearing strategy.

Analysis	Electron smearing	$\not\!\!E_t$ smearing	Acceptance %
$W \rightarrow e\nu$	None	None	37.91
$Z \rightarrow ee$	None	None	31.32
$W \rightarrow e\nu$	MC	None	37.21
$Z \rightarrow ee$	MC	None	30.19
$W \rightarrow e\nu$	None	MC (proc a)	37.82
$W \rightarrow e\nu$	None	Data driven (proc a)	37.48
$W \rightarrow e\nu$	None	MC (proc b)	37.86
$W \rightarrow e\nu$	None	Data driven (proc b)	38.11
$W \rightarrow e\nu$	MC	MC (proc a)	37.14
$Z \rightarrow ee$	MC	N/A	30.19

Tab. 1.2: Computed acceptances including effect of smearing. The statistical uncertainty on the acceptance is 0.1% for $Z \rightarrow ee$ events and 0.08% for $W \rightarrow e\nu$ events.

Table 1.4 shows the effect of systematic uncertainties on the lepton and $\not\!\!E_t$scale and resolution on the calculated acceptances. The central values and associated systematic uncertainties of the scales and resolutions are evaluated in chapter **??** but summarised in table 1.3. Upwards systematic shifts only have been shown but downwards shifts have been seen to give similar results (in the opposite direction). The statistical fluctuations are ignored in this section as they are negligible in comparison to the systematic uncertainties on the method.

Quantity	Scale systematic/%	Resolution systematic/%
Electron	0.2%	0.3%
$\not\!\!E_t$ (ZP_T)	5%	10%
$\not\!\!E_t$ (Anti ZP_T)	N/A%	10%

Tab. 1.3: Summary of detector responses (fractional values shown). Note the fractional scale systematic along the anti ZP_T axis not applicable as the $\not\!\!E_t$ is not scaled in this direction (as there is very little measured scale bias).

Analysis	Electron scale	Electron resolution	$\not\!\!E_t$ scale	$\not\!\!E_t$ resolution	Δ Acceptance %
$W \to e\nu$	central+sys	central	central	central	Negligible
$W \to e\nu$	central	central+sys	central	central	Negligible
$Z \to ee$	central+sys	central	central	central	0.01%
$Z \to ee$	central	central+sys	central	central	0.01%
$W \to e\nu$	central	central	central+sys	central	0.03%
$W \to e\nu$	central	central	central	central+sys	0.2%

Tab. 1.4: Deviation of acceptances when taking into account systematic uncertainties on detector scale and resolutions, from acceptances which are computed from 'centrally smeared' quantities.

1.4 Estimation of systematic uncertainties

1.4.1 Experimental uncertainties

The experimental uncertainties on the acceptance calculate originate from detector response and the choice of the lower boundary cut on M_Z. Systematic estimators were devised to account for uncertainties both on the smearing procedure and those on the measurements of the detector response itself.

Estimators for systematic uncertainty in $Z \to ee$ events:

- Placement of the lower M_Z threshold cut: 0.5%
- Impact of electron scale uncertainty on acceptance: Negligible
- Impact of electron resolution uncertainty on acceptance: Negligible
- Estimated impact of electron smearing procedure on acceptance: %

Estimators for systematic uncertainty in $W \to e\nu$ events:

- Placement of the lower M_Z threshold cut: 0.5%
- Impact of electron scale uncertainty on acceptance: Negligible
- Impact of electron resolution uncertainty on acceptance: Negligible
- Impact of MEt scale uncertainty on acceptance: 0.03%
- Impact of MEt resolution uncertainty on acceptance: 0.2%

- Comparison of acceptance with MC and data driven $\not\!\!E_t$ smearing 0.3%
- Comparison with acceptance between two methods of $\not\!\!E_t$ smearing: 0.04%
- Estimated impact of electron smearing procedure on acceptance: %
- Estimated impact of $\not\!\!E_t$ smearing procedure on acceptance: %

Given the above list, the total systematic uncertainty from these on the acceptances was evaluated at 1% for W and 0.5% for Z events.

1.4.2 Theoretical uncertainties

The theoretical uncertainties on the acceptance are taken from a study by Matthias Schott (cite this) and are evaluated from the same Pythia samples used in this analysis. The systematic originating from the input PDFs was evaluated as well as those from the effects of ISR, intrinsic K_T of the incoming partons, matrix element calculation, underlying event and Photos. The results are summarised in table 1.5.

Effect	Impact on $W \to e\nu$	Impact on $Z \to ee$	Impact on $\Re$
Total	2.44%	2.06%	1.27%

Tab. 1.5: Summary of theoretical percentage uncertainties on the calculated acceptance in Pythia.

1.4.3 Summary of acceptances and associated uncertainties

Table 1.6 summarises the evaluated acceptances along with their associated uncertainties. The statistical uncertainty on $Z \to ee$ and $W \to e\nu$ has been combined in the usual way to obtain the statistical uncertainty on their ratio (needed for a calculation of R) as the two uncertainties are independent of each other. In constrast, the systematic (experimental) percentage uncertainty on the acceptance ratio has been taken to be that from $W \to e\nu$ (the theoretical uncertainty has been determined separately **??**. The reason for doing this is as follows:

- The additional uncertainty on the acceptance ratio to that on the $W \to e\nu$ acceptance would be the additional effect of the $Z \to ee$ smearing.
- To first order, the effect of smearing one electron in $Z \to ee$ will cancel out the effect of smearing the electron in $W \to e\nu$.

- This leaves only the effect of smearing the additional electron in $Z \rightarrow ee$
- This coupled with the uncertainty associated with smearing the $\not\!\!E_t$ in $W \rightarrow e\nu$ means that the total uncertainty should be similar to that associated with smearing the $W \rightarrow e\nu$ event only ($1\times\not\!\!E_t + 1\times$ electron).
- The first order approximation is seen to be valid, given that the effect of electron smearing is a small one compared to some other uncertainties in the analysis.

	$A_{W\rightarrow e\nu}$	$A_{Z\rightarrow ee}$	$A_{Z\rightarrow ee}/A_{W\rightarrow e\nu}$
Acceptance %	37.14	30.19	0.81
Statistical uncertainty %	0.08 (0.22)	0.1 (0.33)	0.005 (0.39)
Systematic uncertainty (experimental) %	1 (2.69)	0.5 (1.66)	0.02 (2.69)
Systematic uncertainty (theory) %	0.77 (2.06)	0.74 (2.44)	0.02 (1.27)

Tab. 1.6: Summary of evaluated acceptances along with associated uncertainties. Absolute values are given with percentage uncertainties in parenthesis.